Angular dependence of the electronic energy loss of 800-keV He ions along the Si⟨100⟩ direction

J. H. R. dos Santos, P. L. Grande, M. Behar, and H. Boudinov
Instituto de Física da Universidade Federal do Rio Grande do Sul, Avenida Bento Goncalves 9500, 91501-970, Porto Alegre, Brazil

G. Schiwietz
Bereich F, Hahn-Meitner-Institut Berlin, Glienicker Strasse 100, D-14109 Berlin, Germany
(Received 12 June 1996; revised manuscript received 11 September 1996)

We present measurements of the stopping power of 800-keV ^{4}He ions channeled along the Si⟨100⟩ axis, as a function of the incidence angle. We compare the experimental results with theoretical calculations by using the impact-parameter-dependent energy loss obtained from the solution of the time-dependent Schrödinger equation through the coupled-channel method. This nonperturbative calculation provides reliable energy-loss results which are in good agreement with the experimental results. [S0163-1829(97)08607-4]

I. INTRODUCTION

The energy loss of energetic ions moving along the major directions of crystals has been studied for many years. In addition to the underlying physics which is involved in the channeling phenomenon, many applications such as studies of atomic surfaces,[1,2] location of foreign atoms,[3,4] defect profiles[5,6] and deep implantation[7] demand accurate knowledge of He stopping powers of channeled ions. However, a full analysis of the stopping of channeled ions turns out to be a complex task because it requires a precise description of both the electronic energy loss as a function of impact parameter for different projectile charge states, and also the ion flux distribution across the channel.

Measurements of the channeling energy loss as a function of the incidence angle provide information on the impact-parameter dependence of the electronic energy loss. There are very few measurements of the angular dependence of the electronic energy loss under channeling conditions.[8,9] All of them were performed at high energies, where the energy losses due to charge-exchange processes are of minor importance. Here we study the angular dependence of the electronic stopping power for channeled ions in silicon from the experimental as well as theoretical points of view with He projectiles at 800 keV. This energy is near the stopping power maximum where charge-exchange processes occur, and only nonperturbative models are able to give reliable energy-loss values.

Early energy-loss models are based on different approaches: the local-density approximation,[10] the local stopping analysis,[11] approximations of first-order theory for inner[12] and outer shells,[13,14] and combinations of these approaches.[9] A full first-order calculation was only recently used to describe the impact-parameter dependence of the electronic energy loss arising from inner-shell ionization of the target.[15] Such a treatment is reliable for light projectiles at velocities large compared to the mean orbital velocities of the target electron involved. Nowadays the computational power has reached a level where such *ab initio* calculations may replace previous semiempirical formulas.[16] Currently there is only one model that yields reliable impact-parameter[17] and scattering-angle[18] dependencies for heavier projectile as well as at lower incident energies (for localized bound states).

The channeled ion trajectories are usually obtained either by analytical models based on the statistical equilibrium assumption,[11] or by Monte Carlo simulations.[19] Both models yield similar results for the ion flux distribution for depths larger than $\approx$100 nm. A full treatment of ion channeling including a reliable energy-loss model, channeled ion trajectories, and projectile charge distributions is still lacking, and this work includes the first steps of such a treatment.

In this paper, we present measurements of the azimuthally averaged energy loss as a function of the ion incidence angle for 800-keV He ions along the Si⟨100⟩ direction by using the backscattering technique described in Ref. 20. The basic principles behind the backscattering experiments are discussed in Sec. II. The results from the axial channeling measurements are presented in Sec. III. We compare our experimental results with theoretical calculations based on an atomic treatment of inner-shell electrons of Si. Since the energy loss to inner-shell electrons is strongly dependent on the trajectory distribution under channeling conditions, a reliable energy-loss model for these electrons must be adopted. Here we use the coupled-channel method[21,22] in order to calculate the impact parameter dependence of the electronic energy loss for each charge state of the He ion in Si. This method is far more precise than the first-order calculations which have mostly been used in the literature. The theoretical procedure (coupled-channel method, charge-exchange treatment and ion flux distribution) used here to describe the angular dependence of channeled stopping power is discussed in Sec. IV. Finally, in Sec. V, the theoretical calculations obtained from the coupled-channel method are presented and compared to the experimental results.

II. EXPERIMENTAL PROCEDURE

In previous experiments, the energy loss of channeled ions has usually been determined by measuring the final energy of the ions transmitted through a thin single crystal. In spite of the many advantages of this method, it strongly de-

pends on the preparation of homogeneous, self-supported, thin single crystals. In order to measure the energy loss for heavy projectiles or even for protons at low energies, extremely thin targets should be employed. This requirement complicates the use of the transmission geometry, and alternative methods have been used in the past.[23,24]

Here we use the experimental procedure described in Ref. 20 for measuring the energy loss under channeling conditions by using the standard Rutherford backscattering technique RBS.[25] We used a SIMOX (separation by implanted oxygen) target[26] from which the channeled energy loss can be obtained almost directly. Besides the energy loss values, the RBS technique simultaneously provides information about the dechanneling that occurs when the ions traverse the sample. Previous results for the energy loss of well-channeled He ions in Si along the $\langle 110 \rangle$ direction[27] have shown that the present backscattering technique yields channeled stopping power values that are consistent with those obtained from transmission experiments.[28]

The SIMOX sample used in the present experiment consisted of a 1500-Å Si$\langle 100 \rangle$ crystal layer on top of a 5000 Å SiO_2 layer on a $\langle 100 \rangle$ Si wafer. The sample was prepared at the IBM T. J. Watson Research Center, New York, and, as revealed by transmission electron microscopy analysis, the interface was sharp (less than 50 Å of roughness), and the interface near region did not show any significant level of extended defects. The sample was thinned by thermal oxidation and chemical etching and, before each RBS experiment, the sample was cleaned and etched using 10% HF to remove the native surface oxide film. The sample was mounted on a three-axis goniometer with a 0.005° precision. The 800-keV He^{2+} beam was produced using the 400-kV ion implanter of the Institute of Physics, Porto Alegre. The He^{2+} beam divergence was less than 0.03° full width.

The measurements were carried out with the beam impinging on the sample at channeling and random directions. In what follows we are going to take as references the $\langle 100 \rangle$ axis ($\Psi = 0$) and the $\{100\}$ plane ($\phi = 0$). Based on a recent study,[29] we have chosen as a random direction the one defined by $\Psi = 6°$ and $\phi = 15°$. For the Si$\langle 100 \rangle$ direction, RBS spectra were recorded for several Ψ angles ranging between $-1.5°$ and $+1.5°$ (in 0.1° steps). In addition, and in order to average out planar channeling effects, we repeated the measurements at five different azimuthal angles ($\phi = 15°$, 26°, 37°, 56°, and 67°). Then we have taken the average value corresponding to each Ψ angle. The backscattered He particles were detected by a Si surface barrier detector placed at 165° with respect to the incident beam. The overall resolution of the detection system was better than 13-keV full width at half maximum.

Typical RBS energy spectra taken with a 800-keV He^{2+} beam at $\Psi = 0.5°$ and 0.7° tilt angles are shown in Fig. 1 together with RBS spectra for random and channeling ($\Psi = 0.0°$) directions. The channeling spectrum shows several features. First, the backscattering minimal yield $\chi_{\min}$ (Ref. 25) corresponding to the near Si surface is $\chi_{\min} = 2.5\%$. Second, the $\chi_{\min}$ which corresponds to the near Si/SiO_2 interface region is $\chi_{\min} = 4\%$. Third, the near Si/SiO_2 interface region does not show indications of the existence of significant number of extended defects. Fourth, the Si/SiO_2 edge is as sharp as the front Si one, if one takes into account the straggling of the particles through the Si film. All these features indicate that (a) the Si film is of very good quality; and (b) the near-interface region is well defined and free of a significant level of linear defects. Both observations are in agreement with transmission electronic microscopy (TEM) results given by the supplier. The edge positions for channeling and random incidence are shown by arrows. They were determined by fitting the corresponding spectra with an algorithm which, in addition to the error function (accounting for particle straggling and detector resolution), contains the Rutherford cross-section dependence with energy. Then the energy loss for well-channeled particles can be straightforwardly obtained by comparing the energy of the edge positions for the normal channeled incidence with that for the random one.[20] However, for increasing incidence angles, the dechanneling part of the beam becomes larger, distorting the profile of channeled ions which are backscattered at the Si/SiO_2 interface. In fact, the energy spectrum of backscattered ions will correspond to the sum of dechanneled and channeled ions, so that the simple analysis considering only the edge positions will not provide precise results. For instance, according to Fig. 1, the energy loss for 0.5° seems to be smaller than the one for 0.0°. In order to circumvent this problem, we have to determine the dechanneling profile and remove it from the original RBS spectrum. This procedure is described in Sec. III and in the Appendix.

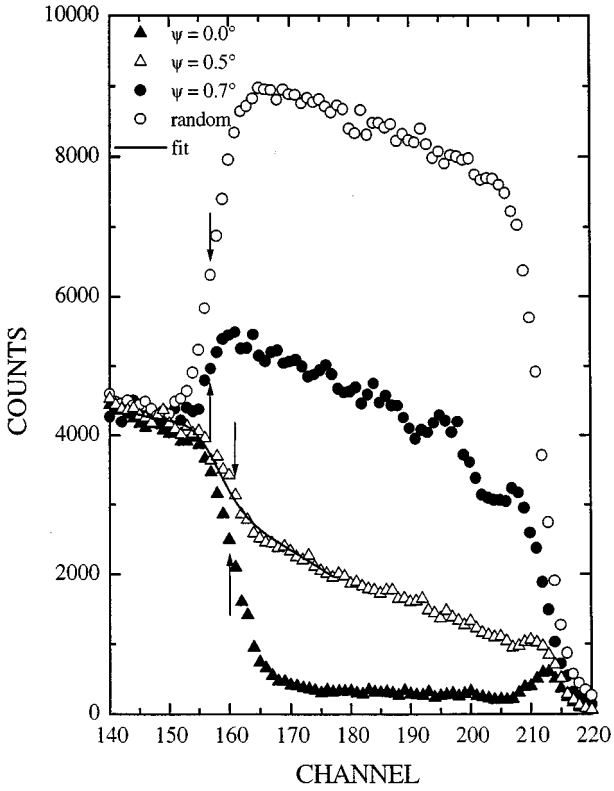

FIG. 1. Random and channeled RBS spectra for $^4He^{2+}$ at 0°, 0.5° and 0.7° about the Si$\langle 100 \rangle$ axis of a SIMOX target taken at 800 keV.

III. DATA ANALYSIS AND EXPERIMENTAL RESULTS

The backscattering of a particle that enters into a channel with an energy E_0 and an angle of incidence Ψ with respect

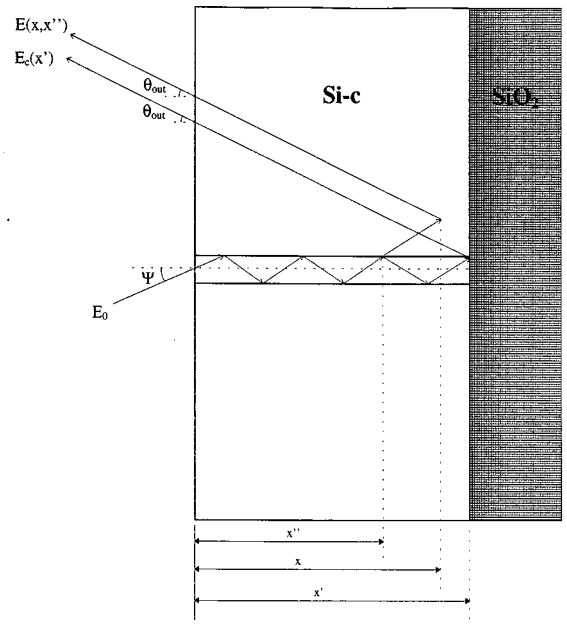

FIG. 2. Schematic representation of two most important contributions to the RBS spectrum. Particles that are backscattered at the Si/SiO_2, and particles that are dechanneled before being backscattered can have the same detected energies. Here x' coincides with the thickness of the film.

to the channel axis will be dominated by two different scattering scenarios:

(a) It can move along the Si⟨100⟩ channel and then be backscattered at a depth x' by defects in the channel or by the Si and O atoms in the SiO_2 layer. It will emerge from the sample at an angle θ_{out} with an energy $E_c(x')$ [see Fig. 2].

(b) It can move in the channel up to a distance between x'' and $x''+dx''$, and then be dechanneled. Still it may go in a forward direction almost parallel to the channel axis and finally, as shown by Fig. 2, it will be backscattered at a distance x, emerging from the sample with the same angle θ_{out} and energy $E(x,x'')$.

The total fraction of backscattered particles with an energy E_1 is given by the contribution of the channeled backscattered particles plus those which are first dechanneled, most likely in a random direction, and then backscattered:

$$f(E_1)=f_c(E_1)+f_d(E_1), \tag{1}$$

with

$$f_c(E_1)=\int_0^\infty dx'[1-\chi(x')]P_{sc}^c(x')\,\delta(E_1-E_c(x')) \tag{2}$$

and

$$f_d(E_1)=\int_0^\infty dx\int_0^x d\chi(x'')P_{sc}(x,x'')\,\delta(E_1-E(x,x'')), \tag{3}$$

where $\chi(x')$ is the fraction of dechanneled particles at the depth x', and $d\chi(x'')$, the fraction of particles dechanneled at the depth between x'' and $x''+dx''$. $P_{sc}(x,x'')$ is the probability of the dechanneled particle being backscattered with a large angle at a depth x, emerging from the sample with an energy $E(x,x'')$ at an angle θ_{out} relative to the normal of the target surface. $P_{sc}^c(x')$ is the probability of a particle being backscattered inside the channel or in the SiO_2 matrix at a depth x' from the surface, and being detected at the angle θ_{out} with an energy $E_c(x')$. Equation (1) has been evaluated by assuming an exponentially decreasing channeling fraction $[1-\chi(x')=\exp(-\lambda x')]$,[30] and using the backscattered probabilities P_{sc} and P_{sc}^c in terms of atomic densities and Rutherford cross sections.[25] In order to determine $E_c(x')$ and $E(x,x'')$ as functions of x', x, and x'', we used the random stopping powers of He in Si and SiO_2 of Refs. 31 and 32. Thus we fitted $f(E_1)$ after convoluting it with the energy straggling and energy resolution of the detection system, to the experimental spectra to obtain (a) the fraction of the dechanneled particles, and (b) the energy loss in the incoming path (channeling). For more details, see the Appendix. It should be stressed that in the fitting procedure there are only two free parameters: the channeled stopping power $(dE/dx)_c$ and λ. In addition we would like to mention that whenever the fraction of the dechanneled particles is less than, e.g., 15%, this analysis yields the same energy-loss value as the one given by the simple error-function-like fitting method.

The solid line in Fig. 1 shows the result of the fitting procedure applied to the RBS spectrum corresponding to $\Psi=0.5°$. In the same way we have obtained for all RBS spectra the channeling stopping power of the He particle as a function of the angle Ψ, and averaged over the azimuthal angle. In addition, we determined the ratio α between the channeled and the random stopping powers. Figure 3 shows these final results after averaging them about the axial direction. As can be observed, the ratio α has a half-width of about 0.4° which is almost half of the value of the corresponding channeling dip (0.7°) obtained from the dechanneling intensity profiles (also shown in Fig. 3). This means that, at large angles of incidence, channeled ions lose as much energy as in a random direction. This feature is a consequence of the different impact-parameter dependencies of the electronic and nuclear energy transfers, and is related to the spatial distribution and the low mass of the electrons.

IV. THEORETICAL PROCEDURE

The angular dependence of the electronic stopping power shown in Fig. 3 is a direct consequence of the impact-parameter dependence of the electronic energy loss. Let Ψ be the entrance angle of the He beam. Then the mean energy lost by the projectile after passing a thickness t through the Si crystal is given by

$$\Delta E(\Psi)=\frac{\int_{\mathcal{A}} d^2\rho\int_0^t dx\frac{dE}{dx}(\vec{\rho})\Phi(\Psi,\vec{\rho},x)}{\int_{\mathcal{A}} d^2\rho\int_0^t dx\Phi(\Psi,\vec{\rho},x)}, \tag{4}$$

where $\mathcal{A}$ is the transversal area of the Si⟨100⟩ channel, $\vec{\rho}$ is the transversal distance ($\vec{\rho}=0$ is the center of the channel), and Φ is the ion flux distribution at the distance $\vec{\rho}$ and depth

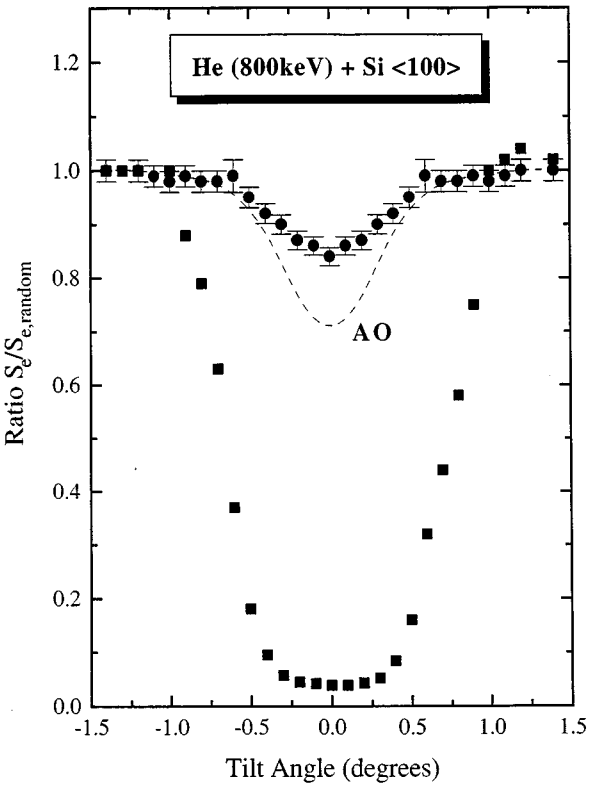

FIG. 3. Ratio α of channeled to random stopping power for 800-keV He ions along the Si$\langle 100\rangle$ direction as a function of the incidence angle. The full circles are the present experimental results, and the dashed curve is the theoretical calculation based on the coupled-channel method. On the same scale the channeling dip (full squares) obtained from the dechanneling profiles is plotted.

x. The energy loss per traversed distance $dE/dx(\vec{\rho})$ may be divided into three contributions,

$$\frac{dE}{dx}(\vec{\rho})=\left(\frac{dE}{dx}(\vec{\rho})\right)_{\text{inner}}+\left(\frac{dE}{dx}(\vec{\rho})\right)_{\text{valence}}+\left(\frac{dE}{dx}(\vec{\rho})\right)_{\text{proj.-}e}. \tag{5}$$

The first contribution corresponds to the energy loss due to inner-shell electrons of the Si atoms. Since these electrons are highly localized, and the corresponding energy loss depends strongly on the transverse distance and may be calculated accurately by considering the contribution of each Si atom.[33] Thus, neglecting any solid-state effects, the first term of Eq. (5) can be evaluated as

$$\left(\frac{dE}{dx}(\vec{\rho})\right)_{\text{inner}}=\frac{Q(b_1)+Q(b_2)+Q(b_3)+Q(b_4)}{d}, \tag{6}$$

where $Q(b)$ is the mean energy transferred to the Si inner-shell electrons (K and L shells). The distance d corresponds to the interatomic distance (5.43 Å) along the $\langle 100\rangle$ Si direction, and b_1, b_2, b_3, and b_4 are the impact parameters relative to the four Si atoms equidistant from the center of the $\langle 100\rangle$ channel. The contributions from other Si atoms are neglected, since they are close to zero.

The second term of Eq. (5) is due to the valence electrons of Si (M shell). These electrons are almost homogeneously distributed. We assume this contribution to be independent of the ion transverse position $\vec{\rho}$. Using the local-density approximation, the spatial variation of the valence-electron contribution was calculated in Ref. 15 for the Si$\langle 100\rangle$ and $\langle 110\rangle$ directions. According to this work, the energy loss across the Si$\langle 100\rangle$ channel is independent of the ion transverse position $\vec{\rho}$ to within 15%, leading to a variation of less than 3% for the ratio in Figs. 3 and 10. This situation is different for the widest channel, $\langle 110\rangle$, where the position dependence of the electronic energy loss due to the valence electrons has to be considered.[15]

Finally, the last term in Eq. (5) corresponds to the energy loss due to projectile ionization and excitation. The incident ion He^{2+} can capture electrons from Si. This process leads to the formation of He^{+}. The energy loss due to this capture process is already accounted for by the first two terms of Eq. (5). However, for projectiles carrying electrons, the projectile ionization and excitation is also a source of energy loss. The energy transfer due to projectile ionization and excitation depends strongly on the impact parameter of the He-Si collision. Consequently, the energy loss per traversed distance $(dE/dx(\vec{\rho}))_{\text{proj.-}e}$ for a Si crystal can also be determined in terms of the mean energy loss as a function of the impact parameter b, similar to Eq. (6). The orbital radius of ground-state He^{+} (the main fraction of He^{+} ions) is small compared to the interatomic distances in Si. Since the velocity is also low enough, coherence effects due to periodicity of the target atoms are expected to be of minor importance.

The electron of the He^{+} ion can be removed due to Coulomb interactions with the Si atoms, producing He^{2+}. After repeated charge-state changing events (after passing just a few monolayers), an equilibrium charge-state distribution is attained. The values of charge-state fractions for channeled He ions in Si at 800 keV can be found in Ref. 34. The charge-state fraction for doubly ionized He ions f_{++} is about 0.65, and for singly ionized He ions f_{+} is about 0.35. The fraction f_0 for He^{0} may be neglected.

Figure 4 shows a sketch of the basic energy-loss processes for a He ion penetrating Si, namely the Si ionization and excitation due to He^{2+} and He^{+} impact, the projectile ionization and excitation due to Coulomb interactions with Si nuclei and electrons, and capture of the Si electrons into unoccupied He states. At high energies, the dominant process is the ionization and excitation of the Si atoms due to He^{2+} impact, which can be accurately described by first-order perturbation theory. However, in the present case (200 keV/amu), only nonperturbative calculations yield reliable energy-loss values. In the case of projectile ionization, first-order calculations overestimate the electron-loss cross section by a factor of 3 (for collisions with Ne atoms at 1000 keV),[35,36] because ionization probabilities do exceed 100% in the case of the heavy target.

In order to obtain the ion flux distribution, we use the string potential model.[37,38] Consequently, only the transverse motion (across the Si$\langle 100\rangle$ channel) has to be determined. For Si$\langle 100\rangle$ axial channeling, four Moliere string potentials[37] were added to calculate the potential energy as a function of position $\vec{\rho}$. We numerically solve Newton's equations of motion for an ensemble of ions impinging on the channel with entrance angle Ψ. Thus the two-dimensional transverse mo-

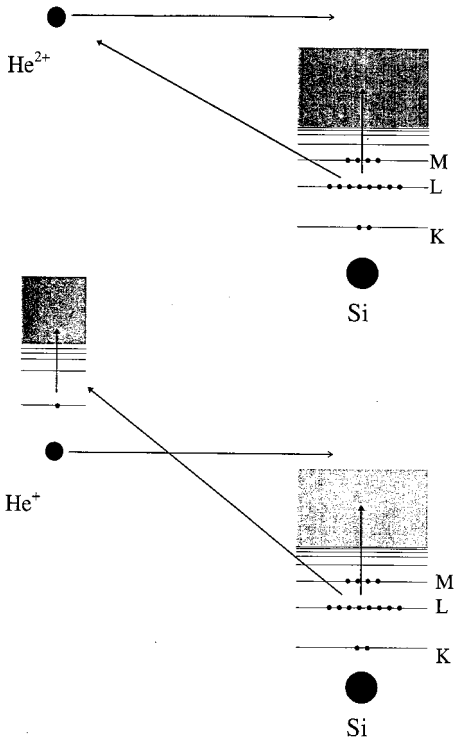

FIG. 4. Diagrammatic representation of the basic energy-loss processes of a He beam colliding with Si atoms.

tion and the ion flux distribution Φ as a function of the penetrated depth were calculated. The ion flux distribution could also be estimated by using the assumption of statistical equilibrium.[11] However, comparisons with the ion flux determined from the numerical solution of Newton's equations show that statistical equilibrium is not achieved for the target thickness used in this work.

The ratio α between the channeled stopping power and the random one can be written as

$$\alpha = \frac{\langle \Delta E \rangle(\Psi)}{\Delta E_{\text{random}}}, \tag{7}$$

where $\langle \Delta E \rangle$ is obtained from Eq. (4) after averaging the energy loss per traversed distance for each charge state distribution f_+ and f_{++}. Here we assume the ion flux distribution Φ to be independent of the projectile charge state for the He^{2+} and He^+ ions, since the ion trajectories are basically determined by the screened potential of Si. ΔE_{random} corresponds to the energy lost by the projectile after passing the target thickness t in a random direction, and was taken from the experimental value of stopping power for He in Si at random incidence.[31]

In the following we describe the calculation of the electronic energy-loss contribution due to Si inner-shell electrons and the projectile electron (for the He^+ fraction), which are responsible for the angular dependence of the channeling stopping power. The energy loss associated with the Si valence electrons is obtained here from the experimental stopping cross section of Ref. 31 by subtracting the contributions from other processes.

Coupled-channel atomic-orbital (AO) method

It is usually assumed that inner-shell excitations can be adequately treated as localized atomic events. It was shown by theoretical grounds in Ref. 33 that all high-energy excitations (inner- and outer-shell ionization) in solids may be treated using atomic-collision models, and that a free-atom model is sufficient to describe energy losses in solids for incident energies above about 10 keV/amu, even when the energy loss is dominated by conduction-band electrons. Here we will focus attention on atomic treatments of the energy-transfer process, putting aside intraband transitions and collective excitations such as bulk and surface plasmons in solid targets.

This calculation[21,22] is based on the impact-parameter method.[39] The projectile following a classical trajectory provides a time-dependent perturbation on the target electrons. Hence the time-dependent Schrödinger equation is solved by expanding the electronic wave function in a truncated basis of states consisting of atomic orbitals. A set of first-order ordinary coupled differential equations for the coefficients originating from this expansion, the so called coupled-channel equations, is integrated numerically along the classical trajectory of the projectile for a given impact parameter b. The independent particle model is adopted for one active electron moving in the electrostatic field due to the nuclei and the other electrons, which is included in a frozen- core Hartree-Fock-Slater framework.

The essence of the present calculation is to solve numerically in time, step by step, the coupled-channel equations in order to obtain the amplitudes $a_{i\to f}$ for transitions from an initial occupied state i to an unoccupied bound or continuum state f after the collision ($t=\infty$). The excitation and ionization probabilities in a collision with impact parameter b are given by

$$P_{i\to f}(b) = \lim_{t\to\infty} |a_{i\to f}(t)|^2. \tag{8}$$

The active electron ground-state wave function ϕ_i and energy E_i, as well as the excited or continuum wave functions $\phi_{i\to f}$ and energies $E_{i\to f}$ (where a hole in the ith shell is left) are calculated by the Hartree-Fock-Slater procedure.[40] Since each excited or continuum state corresponds to a well-defined energy transfer ($\Delta E_{i\to f} = E_{i\to f} - E_i$), the average electronic energy loss due to one electron in the ith shell for a given impact parameter b can be written as

$$Q_i^{P\to T}(b) = \sum_f P_{i\to f}(b)\Delta E_{i\to f}, \tag{9}$$

where P and T correspond to the projectile and target used in the calculations. It is noted that the above sum has to be replaced by an integral in the case of continuum states. The subscript i indicates the occupied initial state, and f the unoccupied bound and continuum states. For He^{2+} projectiles, the average electronic energy loss reads

$$Q_{++}(b) = \sum_i 2\times Q_i^{\text{He}^{2+}\to\text{Si}}(b), \tag{10}$$

where the initial states i correspond to Si K and L shells ($i = 1s, 2s, 2p_x, 2p_y$, and $2p_z$). The factor of 2 corresponds

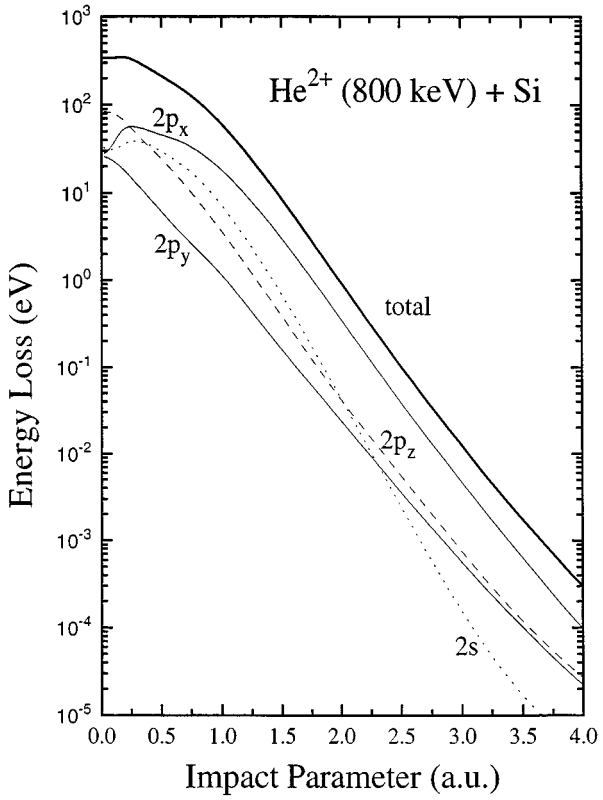

FIG. 5. Impact-parameter dependence of the electronic energy loss for 800-keV He^{2+} colliding with Si atoms calculated with the coupled-channel method. The labels indicate the Si inner shell to which the active electron is initially bound.

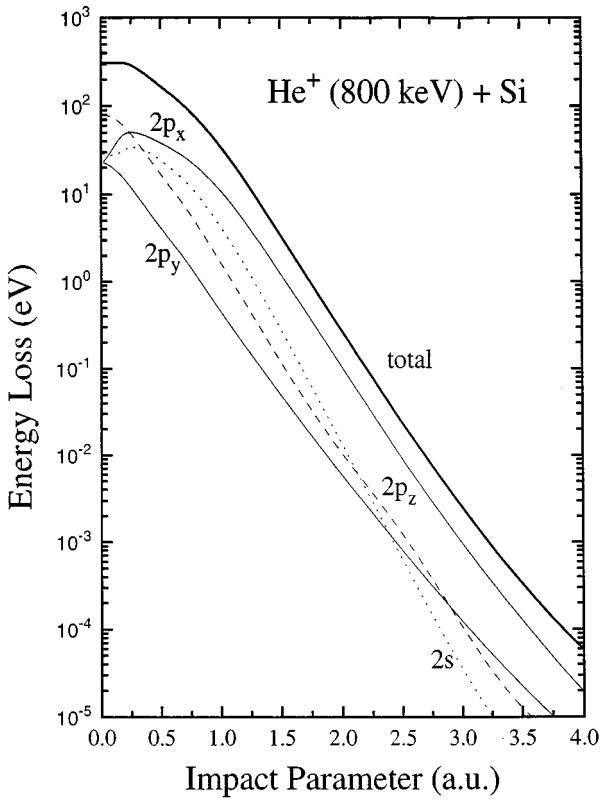

FIG. 6. The same as in Fig. 5, but for He^+ projectiles.

to the number of electrons in the initial orbital i. For the case of singly ionized He^+, the energy loss comes not only from the Si inner-shell electrons, but also from projectile ionization and excitation. Consequently, the mean energy loss for the He^+ fraction is

$$Q_+(b)=\sum_i 2\times Q_i^{He^+\to Si}(b)+Q_{1s}^{Si\to He^+}(b), \qquad (11)$$

and the energy loss averaged over the charge-state distribution is given by

$$\langle Q\rangle(b)=f_+Q_+(b)+f_{++}Q_{++}(b), \qquad (12)$$

which, in connection with Eqs. (5), (6), and (7), provides the angular dependence of the stopping power under channeling conditions. For bare incident ions, the active-electron projectile interaction is just the Coulomb potential. In the case where the projectile carries electrons, the potential seen by the active electron contains not only the Coulomb part due to the projectile-nuclear charge but also the static potential produced by the projectile electrons that screen the projectile nuclear charge. It is emphasized that the calculation of the energy loss due to the projectile electron is performed in a frame where the projectile is at rest. Thus the incoming perturbating particle is the neutral Si atom.

In the present coupled-channel calculations, we used a large number of continuum wave packets (up to 350 ''gerade'' states with partial waves up to $l=8$), since the computation of the electronic stopping power demands high accuracy for the emitted-electron energy spectrum. In addition, the energy loss due to capture into projectile states is naturally included in a large-basis-set calculation. Further details of the calculation, e.g., the numerical treatment of continuum states, adopted basis set, treatment of screened projectiles, may be found in Refs. 21, 22, and 36.

V. THEORETICAL RESULTS AND DISCUSSION

In Figs. 5–7 we present the coupled-channel results for the impact-parameter dependence of the mean energy loss of singly and doubly ionized He ions colliding with Si. The theoretical curves in Figs. 5 and 6 are labeled with the corresponding initial occupied state. The difference between the $2p$ energy-loss curves is related to the spatial orientation of the $2p_x$, $2p_y$, and $2p_z$ orbitals. The contribution of the Si-K shell electrons is negligible, and therefore is not shown in Figs. 5 and 6. The sum of these curves multiplied by the number of electrons in each subshell is represented by a thick solid line, and corresponds to the inner-shell contribution to the energy loss. These contributions are also displayed in Fig. 7 (solid and dashed lines for He^{2+} and He^+, respectively) with the energy loss corresponding to the He^+ projectile ionization and excitation (dashed line). Finally, the averaged energy loss (thick solid line) according to the charge-state distribution [Eq. (12)] is depicted as a function of the impact parameter. Using this curve in Eq. (6), we obtain the mean energy loss per traversed distance as a function of the ion transverse position $\vec{\rho}$ inside the channel.

The ion flux distribution calculated for normal incidence $\Psi=0$ and integrated along the depth (1500 Å) is presented

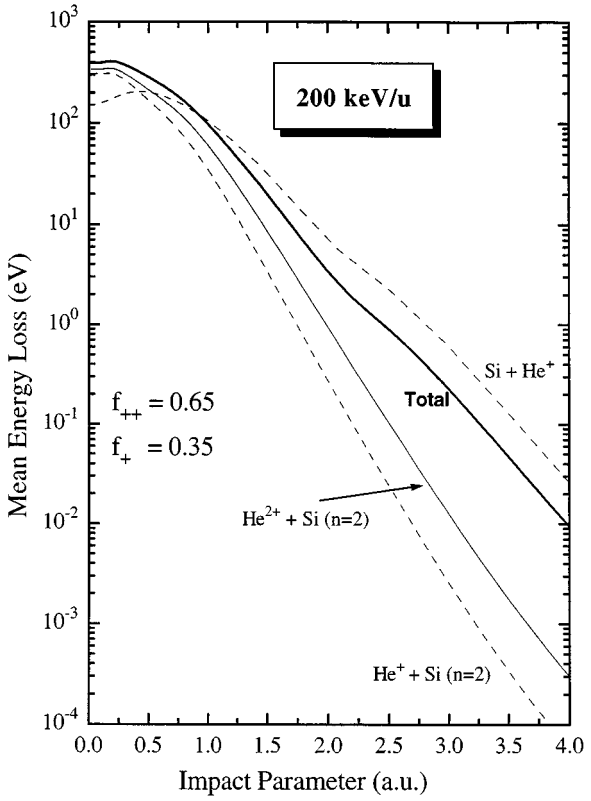

FIG. 7. Coupled-channel results for the impact parameter dependence of the energy loss for He ions colliding with Si atoms. Ionization and excitation of the projectile, in the case of the He^+ charge-state fraction is accounted for by considering the collision system Si + He^+.

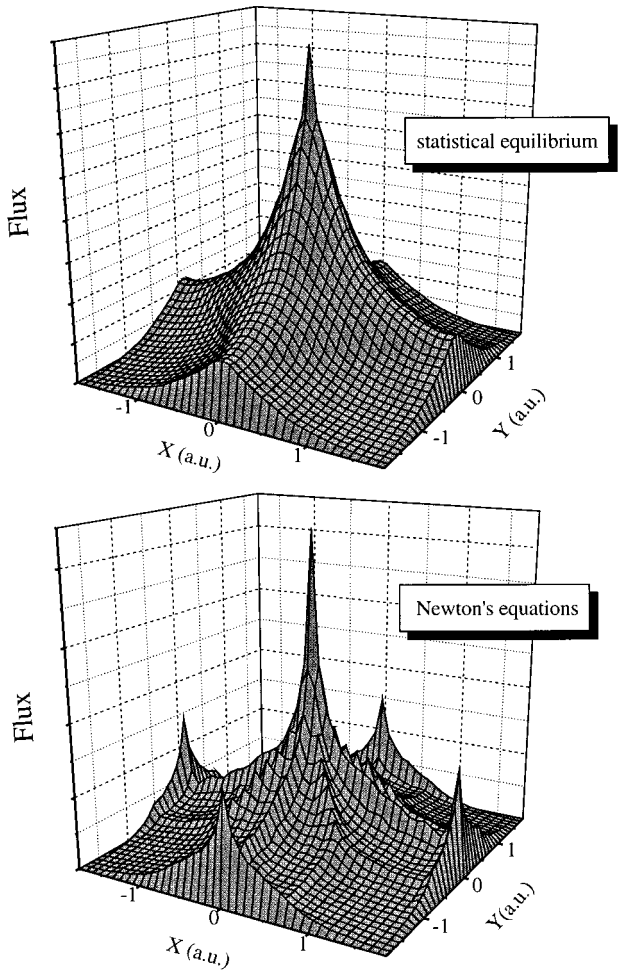

FIG. 8. The flux distribution averaged over 1500 Å of the ions across the Si⟨100⟩ channel.

in Fig. 8. The flux peaking in the center is responsible for the decrease of the channeled ion stopping power, since the energy loss per traversed distance has a minimum at the center of the channel. By increasing the incidence angle Ψ, the flux distribution becomes more uniform. For large angles, the flux distribution is constant like the one for random directions (not shown here). With the angle-dependent flux distribution and the averaged energy loss per traversed distance, we obtain the energy loss as a function of the incidence angle.

The calculated ratio α between the channeled and random energy loss [Eq. (7)] is depicted in Fig. 3 as a dashed line (labeled by AO). Although the calculations predict a half-width similar to that obtained from the experimental results, the value of the ratio α for the normal incidence is underestimated by about 13%. This disagreement comes from the straightforward use of Eq. (4) without considering any experimental and/or theoretical corrections.

Regarding the experimental conditions, some comments can be made. No further cleaning was performed in vacuum, so the deposition of hydrocarbon and the formation of a native oxide layer may influence the ion flux distribution and hence the measurements of energy loss. In a series of auxiliary experiments, the quantity of carbon deposited on the Si surface was estimated. The effect of a maximal quantity of about 20 Å of carbon and 20 Å of amorphous SiO_2 due the formation of native oxide film on the Si⟨100⟩ channel was considered in the calculations. A layer of amorphous material on top of a crystal leads to an angular spreading of the incident ions after penetrating this layer. This angular spreading was calculated with the Monte Carlo simulation TRIM95.[32] The simulated profile of angles Ψ from the crystal axis and the beam divergence were used to calculate the ion flux distribution. The ratio α increases as a consequence of the angular spreading by less than 2% at normal incidence. Other corrections for the ion flux distribution such as inelastic multiple scattering and atomic thermal displacements were also taken into account according to Ref. 37, but they are negligible (less than 1%). The effect of the temperature is also not significant for energy-loss measurements, since the thermal vibrations induce only small changes on the impact-parameter distribution. The averaged electronic energy loss is not sensitive to such small variations.

On the other hand, at a theoretical level, the independent particle model used to take into account all Si inner-shell electrons may strongly overestimate the energy loss in the case of capture events and multiple ionization. Special attention must be drawn to the use of Eqs. (10) and (11) to calculate the total energy loss due to Si inner-shell electrons. The sum of each subshell contribution used in Eqs. (10) and (11) is based on the independent-particle model, and accounts for ionization, excitation, and capture processes.

However, a complete breakdown of the independent-particle model occurs in the case of multiple capture of target electrons into projectile states because the projectile He^+ (He^{2+}) cannot capture more than one (two) electron(s) into the ground state due to the Pauli-exclusion principle. The simple sum of capture probabilities corresponding to each Si inner electron therefore incorporates unphysical capture processes.

In the present calculations, we cannot distinguish the electron capture by the projectile from the ionization process, since we used only target-centered states in the atomic orbital (AO) expansion. In order to obtain the capture contribution to the calculated energy loss, in Fig. 9 we compare the energy loss of He^{2+} ions interacting with the $2s$ Si electron. The solid line corresponds to coupled-channel calculation (AO), and the dashed line represents the energy-loss calculations using the boundary-corrected first-order born approximation[41] for electron capture into the He ground state. The latter calculation takes into account only the capture process in first-order perturbation theory. Both calculations give the same results for impact parameters larger than 0.6 a.u. We can observe two important aspects from this figure. The first one corresponds to the coupled-channel calculation. Even using only target-centered states, this method provides reliable values for capture probabilities as already observed in Ref. 22. Second, the capture process is the main source of energy loss predominating over target inner-shell ionization. For He^+ impact ions, we obtain similar results to the ones shown in Fig. 9. Further evidence of the dominant capture process is a peak around the electron energy corresponding to the capture energy transfer which was observed in the calculated singly differential cross section for collisions of He^{2+} and He^+ with the Si L-shell electrons ($2s$ and $2p$).

Assuming that the capture of Si inner-shell electrons into the He ground state is the dominant energy loss process, we must exclude all unphysical multiple processes in order to obtain more accurate energy-loss values. Thus, for He^{2+} projectiles, we use the following expression to suppress the unphysical multiple-capture processes

$$\begin{aligned} Q^{\text{excl.}}(b) = {} & 2Q_{2s}(b)(1-P_{2s}^{\text{reac.}})(1-P_{2p_x}^{\text{reac.}})^2(1-P_{2p_y}^{\text{reac.}})^2(1-P_{2p_z}^{\text{reac.}})^2 + 2Q_{2p_x}(b)(1-P_{2s}^{\text{reac.}})^2(1-P_{2p_x}^{\text{reac.}})(1-P_{2p_y}^{\text{reac.}})^2 \\ & \times(1-P_{2p_z}^{\text{reac.}})^2 + 2Q_{2p_y}(b)(1-P_{2s}^{\text{reac.}})^2(1-P_{2p_x}^{\text{reac.}})^2(1-P_{2p_y}^{\text{reac.}})(1-P_{2p_z}^{\text{reac.}})^2 \\ & + 2Q_{2p_z}(b)(1-P_{2s}^{\text{reac.}})^2(1-P_{2p_x}^{\text{reac.}})^2(1-P_{2p_y}^{\text{reac.}})^2(1-P_{2p_z}^{\text{reac.}}) + Q^{\text{two-electron}}(b), \end{aligned} \tag{13}$$

with

$$\begin{aligned} Q^{\text{two-electron}}(b) = {} & 2Q_{2s}(b)P_{2s}^{\text{reac.}}(1-P_{2p_x}^{\text{reac.}})^2(1-P_{2p_y}^{\text{reac.}})^2(1-P_{2p_z}^{\text{reac.}})^2 + 2Q_{2p_x}(b)P_{2p_x}^{\text{reac.}}(1-P_{2s}^{\text{reac.}})^2(1-P_{2p_y}^{\text{reac.}})^2(1-P_{2p_z}^{\text{reac.}})^2 \\ & + 2Q_{2p_y}(b)P_{2p_y}^{\text{reac.}}(1-P_{2s}^{\text{reac.}})^2(1-P_{2p_x}^{\text{reac.}})^2(1-P_{2p_z}^{\text{reac.}})^2 + 2Q_{2p_z}(b)P_{2p_z}^{\text{reac.}}(1-P_{2s}^{\text{reac.}})^2(1-P_{2p_x}^{\text{reac.}})^2(1-P_{2p_y}^{\text{reac.}})^2 \\ & + 2(Q_{2s}(b)P_{2p_x}^{\text{reac.}} + Q_{2p_x}(b)P_{2s}^{\text{reac.}})(1-P_{2s}^{\text{reac.}})(1-P_{2p_x}^{\text{reac.}})(1-P_{2p_y}^{\text{reac.}})^2(1-P_{2p_z}^{\text{reac.}})^2 + \cdots, \end{aligned} \tag{14}$$

where $P_i^{\text{reac.}} = \Sigma_f P_{i\to f}$ is the reaction probability, i.e., the sum over ionization, excitation, and capture probabilities for one electron from the ith Si inner-shell. Therefore, $(1-P_i^{\text{reac.}})$ corresponds to the probability of the electron remaining in the ground state. Thus Eq. (13) provides all one- and two-electron processes leading to the energy loss. It is pointed out that the above expression still allows for other double ionization and excitation processes involving an inner-shell electron and a valence-band electron. It is noted that electron capture of valence-band electrons is quite unlikely because of the low orbital velocity in comparison with the projectile velocity and the energy mismatch between target and projectile states.

In the case of He^+ projectiles, we must exclude other than single-electron processes. Moreover, the Pauli principle has to be explicitly taken into account in the case of the capture into the He^+ ground state. In this case, the projectile cannot capture a Si electron with the same spin direction as the projectile electron. Then the energy loss due to capture into He^+ ground state is

$$\begin{aligned} Q(b) = {} & Q_{2s}(b)(1-P_{2s}^{\text{reac.}})(1-P_{2p_x}^{\text{reac.}})^2(1-P_{2p_y}^{\text{reac.}})^2 \\ & \times(1-P_{2p_z}^{\text{reac.}})^2 + Q_{2p_x}(b)(1-P_{2s}^{\text{reac.}})^2(1-P_{2p_x}^{\text{reac.}}) \\ & \times(1-P_{2p_y}^{\text{reac.}})^2(1-P_{2p_z}^{\text{reac.}})^2 + Q_{2p_y}(b)(1-P_{2s}^{\text{reac.}})^2 \\ & \times(1-P_{2p_x}^{\text{reac.}})^2(1-P_{2p_y}^{\text{reac.}})(1-P_{2p_z}^{\text{reac.}})^2 + Q_{2p_z}(b) \\ & \times(1-P_{2s}^{\text{reac.}})^2(1-P_{2p_x}^{\text{reac.}})^2(1-P_{2p_y}^{\text{reac.}})^2(1-P_{2p_z}^{\text{reac.}}). \end{aligned} \tag{15}$$

Thus we have performed corrections on the independent-particle model. In this correction (called AO*), we consider Eq. (13) for the He^{2+} projectiles, and Eq. (15) for the He^+ projectiles. We are assuming only capture into the He^+ ground state, since the capture into projectile excited states are of minor importance.

The energy-loss ratio α calculated by excluding the unphysical capture processes according to the procedure AO* described above is shown in Fig. 10 by a solid line. For

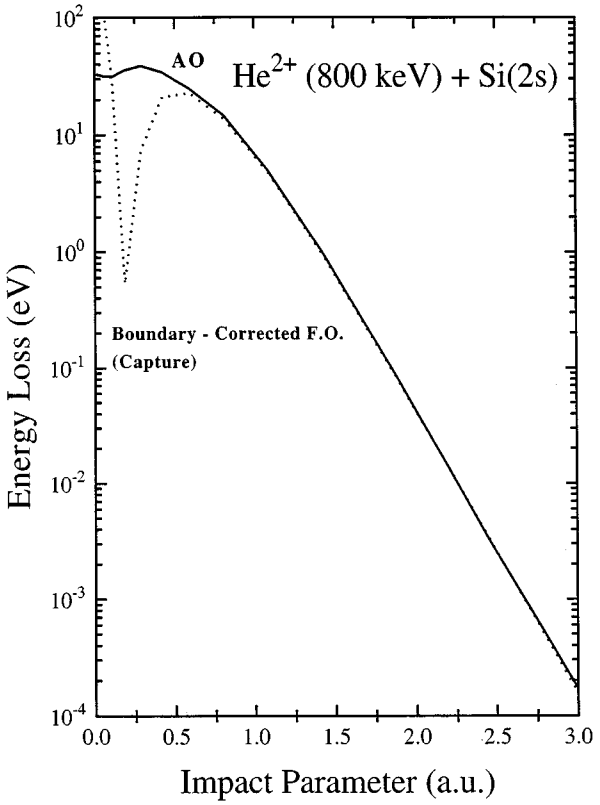

FIG. 9. Comparison between the energy loss due to the Si 2*s* shell calculated from the coupled-channel method with the one obtained for the capture from the Si 2*s* shell into the He^{2+} ground state in the boundary-corrected first-order Born approximation (Ref. 41).

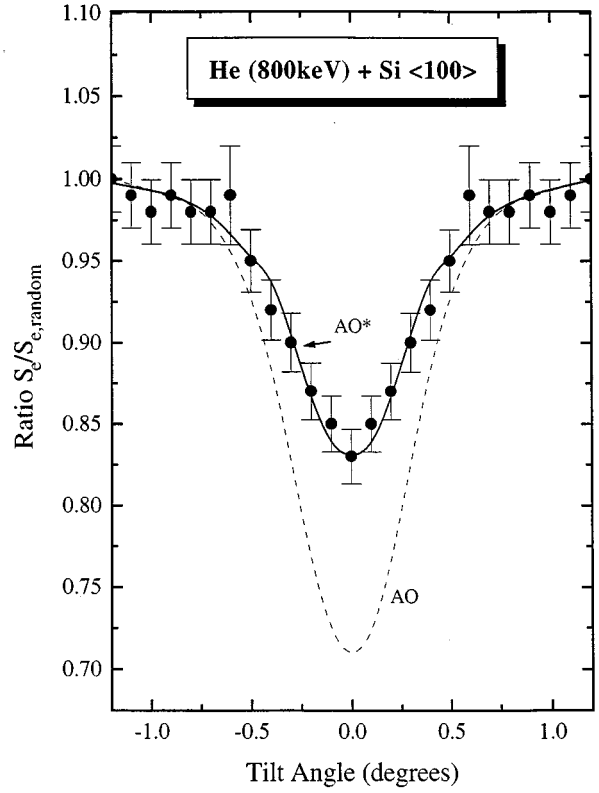

FIG. 10. Ratio α of channeled to random stopping power for 800-keV He ions moving along the Si⟨100⟩ direction as a function of the incidence angle. The full circles and solid line (AO) are taken from Fig. 3. The theoretical curve denoted by AO* is the result of the coupled-channel calculations excluding unphysical capture processes.

comparison, the experimental data from Fig. 3 are also presented with the original AO calculations. A very good agreement is found between the AO* theoretical results and the experimental ones. This figure shows that by excluding the multiple processes involving the Si inner-shell electrons in the coupled-channel results for one electron, we obtain reliable values of the impact-parameter-dependent energy loss.

VI. CONCLUSIONS

In this work we measured and calculated the energy loss of 800-keV He ions channeled along the Si⟨100⟩ axis as a function of the incidence angle. The measurements were performed by using the standard Rutherford backscattering technique on SIMOX targets. A special algorithm was developed in order to analyze the RBS spectra, and extract the channeled component from the raw spectrum. The results show that the ratio α between the channeled and random stopping powers has a half-width of about 0.4°, which is much smaller than the corresponding Si⟨100⟩ channeling dip (0.7°), obtained from the yield of dechanneled He particles. This feature is a direct consequence of the different impact-parameter dependencies of the electronic and nuclear energy transfers.

From the theoretical point of view, a full analysis of the stopping power of channeled particles was performed by considering the impact-parameter-dependent energy loss, projectile charge states, and ion flux distribution. The energy-loss calculations were based on a numerical solution of the coupled-channel equations for each Si inner-shell electron, and also for the projectile electron in the case of singly ionized He projectiles. The independent-particle model was used to obtain the total energy loss.

Near the stopping power maximum (at 800 keV), the angular dependence of the stopping power is basically due to projectile electron loss and capture process from Si inner-shell electrons. The ratio α is well reproduced by coupled-channel calculations by excluding multiple-electron processes involving the Si inner-shell electrons. In this way, very good agreement with the experimental results has been achieved without using any free parameters or further approximations. Moreover, the present results provide tools for a better understanding of the energy loss of ions under channeling conditions.

ACKNOWLEDGMENTS

The numerical work was performed on the Cray YMP-2E at the Supercomputing Center of Universidade Federal do Rio Grande do Sul (CESUP). This work was partially supported by the Brazilian agencies Conselho Nacional de Desenvolvimento Científico e Tecnológico (CNPq) and Financiadora de Estudos e Projetos (FINEP). The authors would also like to thank Dr. D. K. Sadana from the IBM T. J.

Watson Research Center, New York, for supplying the SIMOX samples.

APPENDIX

According to Sec. III, the total fraction of backscattered particles detected with an energy E_1 is given by the contribution of (a) the channeled backscattered particles, and (b) those which are first dechanneled (most likely in a random direction) and then backscattered. In order to evaluate Eq. (2), we first have to obtain

$$E_c(x')=\begin{cases} KE_0-[S_c]x' & \text{for } x'\leqslant t \\ KE_0-[S_c]t-[S]^{\mathrm{SiO_2}}(x'-t) & \text{for } x'>t, \end{cases} \tag{A1}$$

with K being the kinematic factor for Si, E_0 the incident beam energy, t the crystal layer thickness, and with the energy-loss factor

$$[S_c]\equiv \frac{K}{\cos\theta_1}\left(\frac{dE}{dx}\right)_c+\frac{1}{\cos\theta_2}\left(\frac{dE}{dx}\right)_r^{\mathrm{out}} \tag{A2}$$

for the Si layer. Here θ_1 and θ_2 are the angles between the beam and the sample normal and between the sample normal and the detector direction respectively, $(dE/dx)_c$ is the channeled specific energy loss (to be determined), and $(dE/dx)_r^{\mathrm{out}}$, the random one along the outward path (for the present case, $\theta_1=\Psi$ and $\theta_2=\theta_{\mathrm{out}}$). The factor $[S]^{\mathrm{SiO_2}}$ is similar to expression (A2) for the SiO_2 matrix.

The backscattering probability for the channeled fraction of the beam is given by

$$P_{sc}^c(x')dx'=N^c(x')\sigma(E')dx', \tag{A3}$$

σ being the Rutherford backscattering differential cross section, and N^c the density of silicon atoms as seen by the channeled fraction of the ions. The energy E' just before backscattering in this case is

$$E'=\begin{cases} E_0-\left(\dfrac{dE}{dx}\right)_c\dfrac{x'}{\cos\theta_1} & \text{for } x'\leqslant t \\ E_0-\left(\dfrac{dE}{dx}\right)_c\dfrac{t}{\cos\theta_1}-\left(\dfrac{dE}{dx}\right)_{in}^{\mathrm{SiO_2}}\dfrac{x'-t}{\cos\theta_1} & \text{for } x'>t. \end{cases} \tag{A4}$$

We now assume that the differential dechanneling probability $d\chi$ at a depth ξ is proportional to the fraction of channeled particles,

$$d\chi(\xi)=\lambda(1-\chi)d\xi, \tag{A5}$$

where λ is the dechanneling rate.

Using the expressions for $E_c(x')$ [Eq. (A1)], P_{sc}^c [Eq. (A3)], and χ [Eq. (A5)] in Eq. (2) , we obtain the following expression for $f_c(E_1)$:

$$f_c(E_1)=\begin{cases} \dfrac{N_{\mathrm{Si}}^{\mathrm{SiO_2}}}{[S]_{\mathrm{Si}}^{\mathrm{SiO_2}}}\sigma_0\dfrac{e^{-\lambda t}}{\left(1-\dfrac{1}{E_0\cos\theta_1}\left[\left(\dfrac{dE}{dx}\right)_c t+\left(\dfrac{dE}{dx}\right)_{\mathrm{in}}^{\mathrm{SiO_2}}\dfrac{KE_0-E_1-[S_c]t}{[S]^{\mathrm{SiO_2}}}\right]\right)^2} & \text{for } E_1\leqslant KE_0-[S_c]t \\ 0 \quad \text{for } E_1>KE_0-[S_c]t \end{cases} \tag{A6}$$

where $\sigma_0\equiv\sigma(E_0)$ and $N_{\mathrm{Si}}^{\mathrm{SiO_2}}$ is the partial density of Si in SiO_2.

Concerning expression (3), the detected energy of a particle which is dechanneled at x'' and backscattered at $x\geqslant x''$ reads

$$E(x,x'')=KE_0-[S_r]x+K\Delta S_{\mathrm{eff}}x'', \tag{A7}$$

where

$$\Delta S_{\mathrm{eff}}\equiv\frac{\left(\dfrac{dE}{dx}\right)_r^{\mathrm{in}}-\left(\dfrac{dE}{dx}\right)_c}{\cos\theta_1} \tag{A8}$$

for the silicon matrix. The probability of backscattering for the dechanneled fraction of the beam is also given by

$$P_{sc}(x,x'')dx=N(x)\sigma(E)dx, \tag{A9}$$

N being the partial density of Si atoms as seen by the dechanneled fraction of the ions (N_{Si} for the Si layer and $N_{\mathrm{Si}}^{\mathrm{SiO_2}}$ for the SiO_2 matrix),

$$E=E_0-\left(\frac{dE}{dx}\right)_r^{\mathrm{in}}\frac{x}{\cos\theta_1}+\Delta S_{\mathrm{eff}}x''. \tag{A10}$$

After combining Eqs. (A5), (A7), (A9), and (3), we obtain

$$f_d(E_1)=\frac{\exp(\lambda b)\sigma_0}{[S_r]} \times\begin{cases} N_{\mathrm{Si}}^{\mathrm{SiO_2}}\left[I\left(\dfrac{t+b}{c}\right)-I\left(\dfrac{b}{c}\right)\right] & \text{for } E_1<KE_0-[S_r]t \\ N_{\mathrm{Si}}\left[I(t)-I\left(\dfrac{b}{c}\right)\right]+N_{\mathrm{Si}}^{\mathrm{SiO_2}}\left[I\left(\dfrac{t+b}{c}\right)-I(t)\right] & \\ \qquad \text{for } KE_0-[S_r]t\leqslant E_1<KE_0-[S_c]t & \\ N_{\mathrm{Si}}\left[I\left(\dfrac{b}{c-1}\right)-I\left(\dfrac{b}{c}\right)\right] & \text{for } E_1\geqslant KE_0-[S_c]t \end{cases} \tag{A11}$$

where

$$I \equiv \int dx \frac{\exp(-\lambda c x)}{(1-ax)^2}, \tag{A12}$$

$$a \equiv \frac{\left(\frac{dE}{dx}\right)_r^{\text{in}}}{E_0 \cos\theta_1}, \tag{A13}$$

$$c \equiv \frac{[S_r]}{K\Delta S_{\text{eff}}}, \tag{A14}$$

and

$$b(E_1) \equiv \frac{KE_0 - E_1}{K\Delta S_{\text{eff}}}. \tag{A15}$$

After convoluting expressions (A6) and (A11) with the energy straggling and energy resolution of the detection system, we can fit the experimental spectrum and obtain $(dE/dx)_c$ from the fitting procedure. It should be stressed that, in the above fitting procedure, the only free parameters are the channeling stopping power $(dE/dx)_c$ and the (constant) dechanneling rate λ.

[1] L. C. Feldman, P. J. Silverman, J. S. Williams, T. E. Jackman, and I. Stensgaard, Phys. Rev. Lett. **41**, 1396 (1978).

[2] N. W. Cheung, R. T. Culbertson, L. C. Feldman, D. J. Silverman, K. W. West, and J. W. Mayer, Phys. Rev. Lett. **45**, 120 (1980).

[3] W. R. Wampler, Phys. Rev. B **51**, 4998 (1995).

[4] M. A. Boshart, A. A. Bailes, and L. E. Seiberling, Phys. Rev. Lett. **77**, 1087 (1996); J. Vac. Sci. Technol. **13**, 2764 (1995).

[5] *Ion Beam Handbook for Material Analysis*, edited by J. W. Mayer and E. Rimini (Pergamon, Oxford, 1978).

[6] E. Albertazzi, M. Bianconi, G. Lulli, and R. Nipoti, Nucl. Instrum. Methods Phys. Res. Sect. B **118**, 128 (1996).

[7] A. La Ferla, E. Rimini, A. Carnera, A. Gasparotto, G. Ciavola, and G. Ferla, Radiat. Eff. **129**, 133 (1994), and references therein.

[8] H. S. Jin and W. M. Gibson, Nucl. Instrum. Methods Phys. Res. Sect. B **13**, 76 (1986).

[9] A. Dygo, M. A. Boshart, M. W. Grant, and L. E. Seiberling, Nucl. Instrum. Methods Phys. Res. Sect. B **93**, 117 (1994).

[10] J. Lindhard and A. Winther, K. Dan. Vidensk. Selsk. Mat. Fys. Medd. **34**, No. 4 (1964).

[11] J. Lindhard, K. Dan. Vidensk. Selsk. Mat. Fys. Medd. **34**, No. 14 (1965).

[12] K. Dettmann, Z. Phys. A **272**, 227 (1975).

[13] L. R. Logan, C. S. Murthy, and G. R. Srinivasan Phys. Rev. A **46**, 5754 (1992).

[14] P. L. Grande and G. Schiwietz, Phys. Lett. A **163**, 439 (1992).

[15] A. Dygo, M. A. Boshart, L. E. Seiberling, and N. M. Kabachnik, Phys. Rev. A **50**, 4979 (1995).

[16] O. Oen and M. Robinson, Nucl. Instrum. Methods **132**, 647 (1976).

[17] P.L. Grande and G. Schiwietz, Phys. Rev. A **44**, 2984 (1991).

[18] G. Schiwietz, P. L. Grande, C. Auth, H. Winter, and A. Salin, Phys. Rev. Lett. **14**, 2159 (1994).

[19] P. J. M. Smulders and D. O. Boerma, Nucl. Instrum. Methods Phys. Res. Sect. B **29**, 471 (1987).

[20] J. H. R. dos Santos, P. L. Grande, H. Boudinov, M. Behar, R. Stoll, Chr. Klatt, and S. Kalbitzer, Nucl. Instrum. Methods Phys. Res. Sect. B **106**, 51 (1994).

[21] G. Schiwietz, Phys. Rev. A **42**, 296 (1990).

[22] G. Schiwietz and P. L. Grande, Nucl. Instrum. Methods Phys. Res. Sect. B **69**, 10 (1992); P. L. Grande and G. Schiwietz, Phys. Rev. A **47**, 1119 (1993).

[23] G. Götz, K. D. Klinge, and F. Schwabe, Expt. Tech. Phys. **23**, 167 (1975).

[24] F. Cembali and F. Zignani, Radiat. Eff. **31**, 169 (1977).

[25] W. K. Chu, J. W. Mayer, and M.-A. Nicolet, *Backscattering Spectrometry* (Academic, New York, 1978).

[26] K. Izumi, M. Doken, and H. Ariyoshi, Electron. Lett. **14**, 593 (1978).

[27] J. H. R. dos Santos, P. L. Grande, H. Boudinov, and M. Behar, in *Ion Implantation Technology–94*, edited by S. Coffa, G. Ferla, F. Prido, and E. Rimini (Elsevier Science, Amsterdam, 1995).

[28] F. H. Eisen, G. J. Clark, J. Bøttiger, and J. M. Poate, Radiat. Eff. **13**, 93 (1972).

[29] A. Dygo, W. N. Lennard, and I. V. Mitchell, Nucl. Instrum. Methods Phys. Res. Sect. B **84**, 23 (1994).

[30] K. Morita and N. Itoh, J. Phys. Soc. Jpn. **30**, 1430 (1971).

[31] D. Niemann, P. Oberschachtsiek, S. Kalbitzer, and H. P. Zeindl, Nucl. Instrum. Methods Phys. Res. Sect. B **80/81**, 37 (1993).

[32] J. F. Ziegler, J. P. Biersack, and U. Littmark, *The Stopping and Range of Ions in Solids* (Pergamon, New York, 1985).

[33] G. Schiwietz and P. L. Grande, Radiat. Eff. Defects Solids **130**, 137 (1994).

[34] R. J. Petty and G. Dearnaley, Phys. Lett. **50A**, 273 (1974).

[35] M. M. Sant'Anna, W. S. Melo, A. C. F. Santos, G. M. Sigaud, and E. C. Montenegro, Nucl. Instrum. Methods Phys. Res. Sect. B **99**, 46 (1995).

[36] P. L. Grande, G. Schiwietz, G. M. Sigaud, and E. C. Montenegro, Phys. Rev. A **54**, 2983 (1996).

[37] *Channeling: Theory, Observation, and Applications*, edited by D. V. Morgan (Wiley, London, 1973).

[38] D. S. Gemmell, Rev. Mod. Phys. **46**, 129 (1974).

[39] J. Bang and J. M. Hansteen, K. Dan. Vidensk. Selsk. Mat. Fys. Medd. **31**, No. 13 (1959); L. Wilets and S. J. Wallace, Phys. Rev. **169**, 84 (1968); M. R. Flannery and K. J. MacCann, Phys. Rev. A **8**, 2915 (1973).

[40] F. Herman and S. Skillmann, *Atomic Structure Calculations* (Prentice-Hall, Englewood Cliffs, NJ, 1963).

[41] D. P. Dewangan and J. Eichler, J. Phys. B **19**, 2939 (1986); Dz. Belkic, R. Gayet, J. Hanssen, and A. Salin, *ibid.* **19**, 2945 (1986).